Correlations between short- and long-time relaxation in colloidal supercooled liquids and glasses

Chandan K. Mishra, Xiaoguang Ma, Piotr Habdas, Kevin B. Aptowicz, and A. G. Yodh

Phys. Rev. E **100**, 020603 — Published 28 August 2019

DOI: 10.1103/PhysRevE.100.020603

Correlations Between Short- and Long-time Relaxation in Colloidal Supercooled Liquids and Glasses

Chandan K. Mishra,[1,*] Xiaoguang Ma,[1] Piotr Habdas,[2] Kevin B. Aptowicz,[3] and A. G. Yodh[1]

[1]*Department of Physics and Astronomy, University of Pennsylvania, Philadelphia, Pennsylvania 19104, USA*
[2]*Department of Physics, Saint Joseph's University, Philadelphia, Pennsylvania 19131, USA*
[3]*Department of Physics and Engineering, West Chester University, West Chester, Pennsylvania 19383, USA*

(Dated: August 7, 2019)

Spatiotemporal dynamics of short- and long-time structural relaxation are measured experimentally as a function of packing fraction, ϕ, in quasi-two-dimensional colloidal supercooled liquids and glasses. The relaxation times associated with long-time dynamic heterogeneity and short-time intracage motion are found to be strongly correlated and to grow by orders of magnitude with increasing ϕ towards dynamic arrest. We find that clusters of fast particles on the two timescales often overlap, and, interestingly, the distribution of minimum-spatial-separation between closest *non-overlapping* clusters across the two timescales is revealed to be exponential with a decay length that increases with ϕ. In total, the experimental observations suggest short-time relaxation events are very often precursors to heterogeneous relaxation at longer timescales in glassy materials.

Two-step structural relaxation is a hallmark feature of supercooled liquids and glasses that characterizes the spatiotemporal dynamics of disordered packings [1]. The first step, called $\beta-$relaxation, is associated with particle motion within cages formed by their neighbors. The second step, often called $\alpha-$relaxation, is associated with cage rearrangements and cage escape. While experiment, theory, and simulation have revealed that $\alpha-$relaxation in supercooled liquids and glasses is heterogeneous and cooperative [1–12], much less is known about the microscopic underpinnings of $\beta-$relaxation processes. Inhomogeneous mode coupling theory predicts [13], and simulation based on finite-size-scaling arguments [14] suggest, that $\beta-$relaxation (*i.e.*, motion within the cage) should be cooperative. These conjectures, however, are unexplored in experiment. Only a few experiments have focused on the $\beta-$relaxation, and none have considered the possible spatial correlations between $\beta-$relaxation and $\alpha-$relaxation rearrangement clusters, nor the evolution of these correlations upon approach of dynamic arrest.

Nevertheless, important work establishing connections between processes across timescales has been done [13–28]. Experiments on molecular glasses suggest τ_β, the timescale associated with $\beta-$relaxation, is correlated with τ_α, the timescale associated with $\alpha-$relaxation. Many of these experiments are in close agreement with the coupling model of Ngai ($\tau_\alpha \propto \tau_\beta^{1/(1-n)}$, where n is the system-dependent coupling parameter) [15–19]. Other models, with different underlying physics, such as mode coupling theory (MCT) [29] and the quasi-point defect model [30], also predict relationships between the two distinct macroscopic timescales, but the power-law exponent differs among models. Therefore, systematic experiments that probe spatiotemporal structural correlations between relaxation processes at the two distinct timescales are desirable. Colloidal supercooled liquids and glasses offer an excellent model system to elucidate these phenomena with single-particle resolution upon approach of dynamic arrest.

In this communication, we experimentally investigate these phenomena by measuring the spatiotemporal dynamics associated with short- and long-time structural relaxation as a function of packing area fraction, ϕ, in a series of quasi-two-dimensional binary-sphere colloidal supercooled liquids and glasses. We find that τ_β scales as a power law with some well-known timescales associated with long-time dynamic heterogeneity (but not τ_α); the power-law exponent agrees with MCT predictions. Moreover, the spatial distribution of dynamic heterogeneities at short and long timescales is indicative of strong correlations between short- and long-time relaxation events. These correlations, which grow with increasing dynamic arrest, are revealed by the spatial overlap of fast-moving particle clusters at long and short times and by a new, packing-fraction-dependent length scale associated with *non-overlapping* clusters at the two timescales. Taken together, the observations provide evidence that motions "beyond" the nearest-neighbor cage, are spatiotemporally correlated with short-time displacements "within" the cage.

The experiments employ binary particle suspensions of small and large polystyrene spheres with diameters $\sigma_s = 1.0$ μm and $\sigma_l = 1.3$ μm, respectively. This choice of diameter ratio, with a particle number ratio of approximately one, prevents crystallization. The aqueous colloidal suspensions were loaded into a wedged-shaped cell, and the cell was then oriented vertically to induce particle sedimentation into a quasi-two-dimensional (quasi-2D) region within the cell. When the desired packing area fraction, ϕ, was obtained, the cell was left horizontal on the microscope stage to equilibrate for 3-5 hours. We ensured that aging effects measured over the experimental duration are negligible in all samples (see Supplemental Material [31]).

For each ϕ, the trajectories of all particles were measured by video optical microscopy using a 100X oil im-

mersion objective (NA = 1.4) at a frame rate of 4 fps. Depending on ϕ, the experimental data acquisition time varied from 25 to 50 minutes. Particle center-of-mass was tracked using MATLAB, and data was analyzed using standard MATLAB and Python codes [32]. ϕ was estimated using $\phi = [N_s\pi(\frac{\sigma_s}{2})^2 + N_l\pi(\frac{\sigma_l}{2})^2]/A$, where N_s and N_l represent the number of small and large particles in the field-of-view, respectively, and A is the total area of the field-of-view. The range of ϕ was $0.56 \leq \phi \leq 0.81$, and $\frac{N_s}{N_l} = 1.00 \pm 0.10$. Note, this wide range of packing fractions spans from liquid to the deeply supercooled liquid regime (Fig. 1, Fig. 2), and the highest area fraction (= 0.81) is very close to the MCT crossover area fraction [33].

A traditional way to quantify dynamics utilizes the ensemble-averaged particle mean-squared displacement (MSD), $\langle \Delta r^2(t) \rangle = \langle \frac{1}{N} \sum_k^N (\vec{r}_k(t+t_0) - \vec{r}_k(t_0))^2 \rangle$. Here, N is the total number of particles, $\vec{r}_k$ is the position of k^{th} particle, and $\langle\rangle$ denotes an average over all particles for all initial times, t_0, and the lag time, t. Figure 1(a) shows the temporal evolution of the measured MSD for various ϕ. The inflection point in the MSDs at short times defines the short-relaxation time, τ_β [14, 20, 23]. It is apparent as an early-time minimum in the plot of $d\ln(\langle \Delta r^2(t) \rangle)/d\ln(t)$ versus t (Fig. 1(b)). Roughly, τ_β corresponds to the time at which particle motion is limited by the cage formed by its neighbors, *i.e.*, the time at which the particle "feels" its cage. The inset of Fig. 1(b) shows τ_β increasing with ϕ. Note, when $\phi \geq 0.79$, the MSDs remain predominantly subdiffusive over the entire experiment duration, and the curves of $d\ln(\langle \Delta r^2(t) \rangle)/d\ln(t)$ versus t exhibit broad minima. Thus, error bars associated with τ_β grow with increasing ϕ.

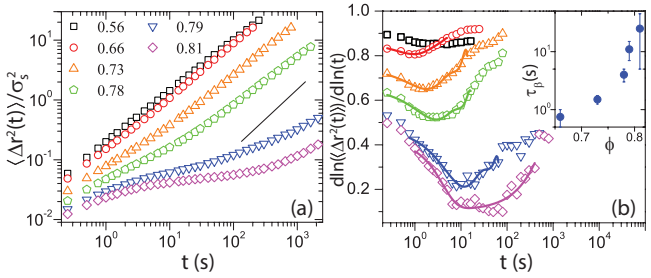

FIG. 1: (a) Log-log plot of the MSD, $\langle \Delta r^2(t) \rangle$, versus lag time t for different ϕ. $\langle \Delta r^2(t) \rangle$ is scaled by the square of the small sphere diameter, σ_s. The solid black line has unit slope. (b) Derivative of the logarithm of $\langle \Delta r^2(t) \rangle$ with respect to logarithm of time, $\frac{d\ln\langle \Delta r^2(t) \rangle}{d\ln(t)}$, versus t at various ϕ. The symbol and color code for ϕ are the same as (a). Solid colored lines are polynomial fits to the data near the minima. Inset shows variation of τ_β with ϕ. Note, the lack of clear minimum at $\phi = 0.56$ prevented estimation of its τ_β.

For spatiotemporal dynamics at longer timescales, the definitions of relaxation time are less standard. Therefore, we quantify long-time structural relaxation using three different methods (Fig. 2). The first approach employs the self-intermediate scattering function, defined as $F_s(\vec{q}, t) = \frac{1}{N}\langle \sum_k^N \exp(i\vec{q} \cdot \vec{r}_k(t+t_0) - \vec{r}_k(t_0)) \rangle$, where $\vec{q}$ is the spatial wavevector. Herein we choose $\vec{q}$ to have magnitude $q = 2\pi/\sigma_s$, where σ_s corresponds to the first peak position in the radial pair-correlation function, $g(r)$, of the sample. Figure 2(a) shows the temporal evolution of $F_s(q,t)$ for various ϕ. Notably, for $\phi \geq 0.66$, the long-time decay of $F_s(q,t)$ has a stretched-exponential form, *i.e.*, $F_s(q,t) \propto \exp -(t/\tau)^\beta$ with $\beta < 1$ (Fig. 2(a)). By convention, the time at which $F_s(q,t)$ decays by $1/e$ is called the long-time structural relaxation time, τ_α [34, 35]. τ_α increases with increasing ϕ (Fig. 2(d)). The stretched-exponential decay of $F_s(q,t)$ at long lag times is indicative of heterogeneous relaxation dynamics, a key feature of glass-forming liquids [1, 35]. Unfortunately, $F_s(q,t)$ lacks information about the times when relaxation dynamics are most heterogeneous. For this reason, we employ two other well-known algorithms to better characterize heterogeneous relaxation dynamics at long times. These schemes yielded relaxation times wherein dynamic heterogeneities are most apparent, which were somewhat different than τ_α.

The first of these (less traditional) methods utilizes the four-point susceptibility $\chi_4(\Delta a, t)$ [7, 36–38]. This function quantifies the temporal variance of the two-point self-correlation function, $Q_2(\Delta a, t)$: $\chi_4(\Delta a, t) = N(\langle Q_2(\Delta a, t)^2 \rangle - \langle Q_2(\Delta a, t) \rangle^2)$. Here, $Q_2(\Delta a, t) = \frac{1}{N}\sum_k^N \exp \frac{-(\vec{r}_k(t+t_0) - \vec{r}_k(t_0))^2}{2\Delta a^2}$, Δa is a pre-selected probing length scale, and the other symbols have their usual meanings. $\chi_4(t)$ measures the non-Gaussian contribution to the dynamics and is largest in the vicinity of the time, τ_4; at τ_4, the dynamics are most heterogeneous (Fig. 2(b)). Note, the peak-amplitude, $\chi_4(\tau_4)$, strongly depends on the probing length scale, Δa (see Supplemental Material [31]). Therefore, in Fig. 2(b) we plot $\chi_4(t)$ versus lag time for each ϕ using the values of Δa that maximize $\chi_4(t)$. The variation of both $\chi_4(\tau_4)$ (Fig. 2(b)) and τ_4 (Fig. 2(d)) with ϕ show that increased supercooling causes structural relaxation to become increasingly heterogeneous and slow.

The final analysis scheme involves direct visualization of the dynamic heterogeneities. We first pick the top 10% most-mobile particles in the sample, *i.e.*, associated with each lag time t. Then we identify particle clusters of most-mobile particles based on nearest neighbor distances (see Supplemental Material [31]). These clusters of most-mobile particles are believed to facilitate structural relaxation in supercooled liquids and glasses [1, 3, 4, 35]. To determine the time when the dynamics are most heterogeneous, we measure the temporal evolution of the mean-cluster-size ($\langle N_c(t) \rangle$) of the most-mobile particles. $\langle N_c(t) \rangle = \frac{\sum_{N_c} N_c^2 P(N_c)}{\sum_{N_c} N_c P(N_c)}$, where $P(N_c)$ is the probability of finding a cluster of size N_c (Fig. 2(c))

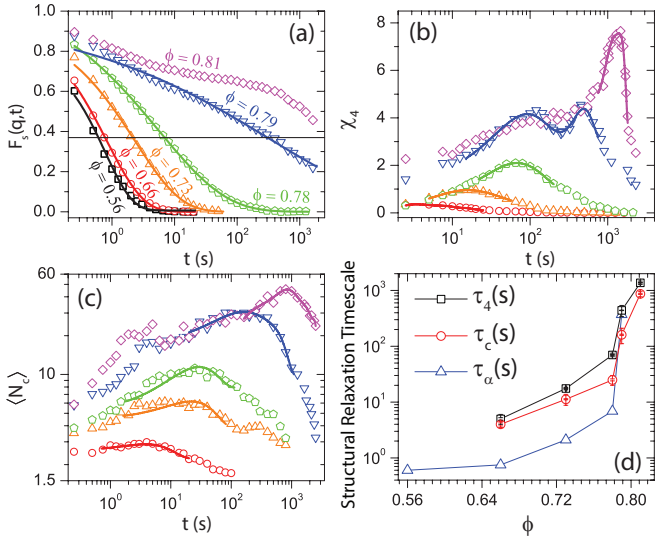

FIG. 2: (a) Self-intermediate scattering function $F_s(q,t)$ plotted versus lag time t for different ϕ. The solid lines are stretched exponential fits, *i.e.*, $\exp(-(t/\tau_\alpha)^\beta)$. The black horizontal line is drawn at $F_s(q,\tau_\alpha) = 1/e$; its intersection with $F_s(q,t)$ determines τ_α. (b) Four-point susceptibility $\chi_4(t)$, with probing length scale (Δa) chosen to maximize χ_4, versus lag time t at each ϕ. (c) Mean cluster size of the top 10% of the most-mobile particles, $\langle N_c(t)\rangle$, plotted versus lag time t for different ϕ. The symbols and color code for ϕ are the same as in (a)-(c). Since dynamic heterogeneities are absent at the lowest packing fraction ($\phi = 0.56$), the long-time relaxation timescales, τ_4 and τ_c, were not estimated for the lowest packing fraction in (b) and (c), respectively. Solid lines in (b) and (c) are polynomial fits to the data near the peak. (d) Long-relaxation timescales τ_4 (squares), τ_c (circles), and τ_α (triangles) versus ϕ.

[3, 4]. The time at which $\langle N_c(t)\rangle$ peaks is τ_c; τ_c defines the time at which the heterogeneous dynamics are most prominent within this scheme. Figure 2(c) is thus analogous to Fig. 2(b). Similar trends with respect to packing (ϕ) are observed for $\langle N_c(\tau_c)\rangle$, τ_c, and $\chi_4(\tau_4)$, τ_4, respectively. Notice, for fixed ϕ, the trends in Fig. 2(d) show that τ_c is always slightly less than τ_4.

Next, we examine how the three long-time relaxation timescales, *i.e.*, τ_4, τ_c, τ_α, vary as a function of the short-time relaxation time, τ_β. Figure 3 shows this variation. All three long-time relaxation timescales increase monotonically with τ_β. Clear power-law scaling between τ_α and τ_β is not evident in Figure 3. This finding differs from early experimental work based on dynamic light scattering from 3D colloidal systems that suggested a power-law relation between τ_α and τ_β with an exponent consistent with the MCT predictions [28]; *i.e.*, $\tau_\alpha \propto \tau_\beta^{(1+\frac{a}{b})}$, wherein a and b are mode coupling exponents [29]. Note, however, τ_β was not measured directly in [28]; rather, it was inferred using MCT predictions. By contrast, spatiotemporal information from optical microscopy permits experimental determination of three long-time structural relaxation timescales, τ_α, τ_4, and τ_c, and the latter two timescales are sensitive to long-time dynamic heterogeneities. Interestingly, when using all ϕ data, both the τ_4, and τ_c timescales exhibit power-law scaling versus τ_β, albeit over our limited experimental dynamic range. Moreover, the exponent (~ 1.5) is in concordance with MCT predictions; for our system $a = 0.32 \pm 0.01$ and $b = 0.61 \pm 0.02$ [33]. These findings could enable estimation of long-time dynamic heterogeneity timescales (τ_c and τ_4) from information about short-timescale relaxation (τ_β) and vice versa, but it requires further study and explanation.

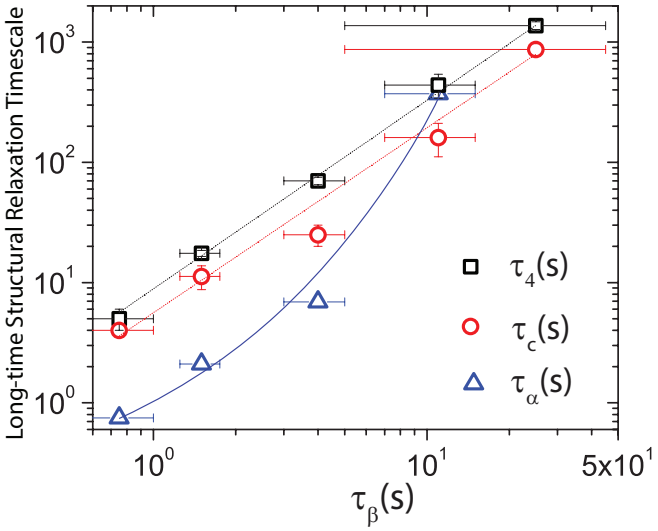

FIG. 3: Log-log plot of τ_4 (squares), τ_c (circles), and τ_α (triangles) versus short-relaxation time (τ_β). The black and red lines are fits that suggest power-law scaling and have a slope of ~ 1.5. The blue line is to guide the eye for τ_α.

The observation of power law scaling between long-time dynamic heterogeneity timescales (τ_c, τ_4) and τ_β prompted us to investigate possible spatial correlations of relaxation dynamics across the timescales (τ_c versus τ_β). To this end, we chose the top 10% of the most-mobile particles associated for lag times of τ_c and τ_β, and we identified all associated particle clusters [3, 4, 35]. Figure 4(a) and (b) show single snapshots of clusters of most-mobile particles at $\phi = 0.73$ and $\phi = 0.79$, respectively. The sizes of the both τ_c- and $\tau_\beta-$clusters increase with ϕ, and at a fixed area fraction, the mean size of the $\tau_\beta-$clusters is smaller than that of the τ_c-clusters (Fig. 2(c), Fig. 4(a) and (b)).

We quantified the morphology of both τ_c- and $\tau_\beta-$clusters. The morphology of τ_c-clusters has been investigated in prior experiments [3, 4, 35, 39]. Here, consistent with these works, we observed them to become increasingly compact as the samples become more dynamically arrested (see Supplemental MAterial [31]). By contrast, the structural relaxation and corresponding morphology of $\tau_\beta-$clusters has never been probed. Inter-

estingly, the $\tau_\beta-$clusters are string-like at low ϕ, and they become predominantly compact at higher ϕ (see Supplemental Material [31]). In total, the observations suggest that both short-time (intra-cage motions) and long-time (inter-cage motions) structural relaxation are heterogeneous and cooperative in nature.

Finally, we explore the spatial correlations between τ_c- and $\tau_\beta-$clusters. In Fig. 4(a) and (b), we exhibit these mobile clusters for a single frame on both long- and short-timescales at two different ϕ. While it is difficult for us to measure the temporal trajectory of $\tau_\beta-$cluster(s) as they evolve and potentially contribute to the generation of τ_c-cluster(s), we can explore other types of connections between the spatial distribution of clusters of most-mobile particles across the τ_β and τ_c timescales (*i.e.*, for fixed initial time t_0).

Recent two-dimensional numerical simulations suggest the potential for overlap of short-time clusters of fast particles (quantified by particle Debye-Waller factor) with clusters of mobile particles at longer timescales [26]. To investigate this notion systematically with ϕ, we first measured the overlap fraction of τ_c-clusters with respect to $\tau_\beta-$clusters. Here, an overlap is defined to occur whenever a τ_c-cluster shares at least one of its particles with those in a $\tau_\beta-$cluster. Interestingly, the fraction of overlapping clusters increases with increasing packing fraction (Fig. 4(c)). This observation suggests that the parts of the sample that relax at long-time (τ_c-clusters) are fairly likely to include fast-cluster regions at shorter timescales ($\tau_\beta-$clusters); moreover, the probability for interaction across timescales increases on approaching dynamic arrest. In other words, relaxation at the two distinct timescales appears to be correlated, and this correlation becomes stronger with increasing ϕ. Note, experimental work in granular systems has also probed spatial structure of short- and long-time dynamics [40]; this work used instantaneous hopping events (only) as the quantifier for dynamic heterogeneities. Our approach is different in that it focuses on continuous particle displacements that include both hopping and diffusive motions that occur during the short- (τ_β) and long-time (τ_c) windows. The hop-only analysis is limited to deeply supercooled liquids and glassy samples (with relaxation via activated hops). Our approach is in line with some well-established notions about dynamic heterogeneities [1, 3, 4, 35] and can be applied to particulate systems at lower packing fractions which relax via diffusive cage-rearrangements.

A closer examination of these cluster images reveals that full overlap of a $\tau_\beta-$cluster with a τ_c-cluster is rare (Fig. 4(a) & (b), see Supplemental Material [31]). This observation suggests that $\tau_\beta-$clusters in the vicinity of τ_c-clusters, but not overlapping, could also facilitate relaxation at long timescales. To explore this hypothesis quantitatively, for each $\tau_\beta-$cluster, we measure the minimum particle-to-particle distance to the closest τ_c-cluster, *i.e.*, the distance $d_{\beta c}^{\min}$. Interestingly, we discovered the probability distribution of $d_{\beta c}^{\min}$, *i.e.*, $P(d_{\beta c}^{\min})$, to be exponential with a unique decay length for each ϕ (Fig. 4(d)). The exponential distribution facilitates extraction of a characteristic lengthscale, ξ, which offers a novel way to quantify the extent to which spatiotemporal dynamics at short-time facilitate cage rearrangement and structural relaxation at longer timescales. Notice, ξ increases significantly with increasing ϕ (Fig. 4(e)). These observations suggest that clusters of the most-mobile particles at short-time help to facilitate cage-rearrangement/escape at long time, even when interact-

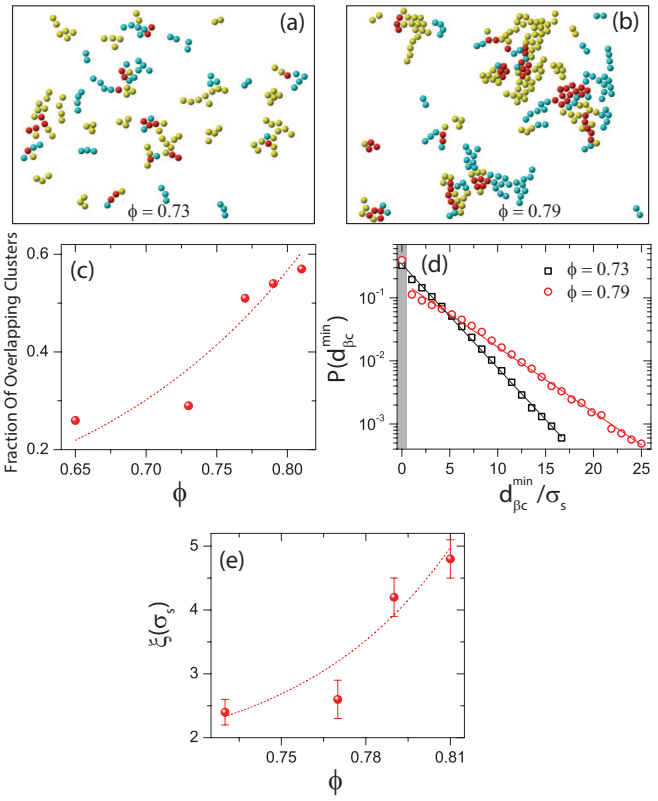

FIG. 4: Single-frame snapshots of clusters of the top 10% most-mobile particles at lag times τ_β (blue spheres) and τ_c (yellow spheres) for (a) $\phi = 0.73$ and (b) $\phi = 0.79$. Particles that are "most-mobile" at both τ_β and τ_c are shown as red spheres. Note, at a fixed area fraction, the mean size of the $\tau_\beta-$clusters is smaller than that of the τ_c-clusters. (c) The fraction of τ_c-clusters that overlap with $\tau_\beta-$clusters versus packing fraction ϕ (see the text for overlap definition). (d) The normalized probability distribution of the minimum-spatial-separation (MSS) between the closest non-overlapping τ_c- cluster with respect to each $\tau_\beta-$ cluster, *i.e.*, $P(d_{\beta c}^{\min})$ versus $d_{\beta c}^{\min}$ at $\phi = 0.73$ (squares) and $\phi = 0.79$ (circles). The grey shaded bin corresponds to $d_{\beta c}^{\min} = 0$ *i.e.* overlapping $\tau_\beta-$ and τ_c-clusters. Solid black and red lines are exponential fits to the probability distribution data. Here, $d_{\beta c}^{\min}$ is normalized by small particle diameter σ_s. (e) The exponential decay length, $\xi(\sigma_s)$, of the probability distributions (for example, (d)) versus ϕ. The red-dashed lines in (c) and (e) guide the eye.

ing over a comparatively long (many particle) length scale; moreover, ξ grows as the glass transition is approached. ξ should not be confused with the heterogeneity lengthscale at *only* long-times that is suggested in the Adam-Gibbs hypothesis [9]; rather, here we are exploring the cooperativity of relaxation *across* different timescales as the glass transition is approached. Note also, this relationship of ξ versus ϕ might be expected to be blurred to some degree by multiple features such as the cluster number, cluster size, and cluster morphology, which also evolve with ϕ and that are difficult to control for (see Supplemental Material [31]).

While prior studies have explored the scaling relation between τ_α and τ_β [16–19, 23], the present work is unique because it experimentally exhibits, with single-particle resolution, the correlations between relaxation processes at different timescales and it identifies a spatial correlation between them. We find that relaxation events at short timescales (τ_β) appear to be precursors to those at longer times (τ_c). The increase with ϕ, of both the overlap fraction of τ_c-clusters with $\tau_\beta-$clusters and the length scale, ξ, is consistent with the notion that cooperative motion of particles increases upon approaching dynamic arrest; this notion is also reflected in the trend of $\chi_4(t_4)$ and $\langle N_c(\tau_c)\rangle$ with ϕ (Fig. 2(b), (c)).

In summary, we have studied spatiotemporal relaxation on multiple timescales in colloidal glass precursors. We observe power law scaling over two decades of dynamic range between the timescales associated with long- versus short-time spatiotemporal relaxation and the observed power law exponent agrees with MCT. The results suggest that short-time structural relaxation can provide useful information about long-time structural relaxation and vice versa. Interestingly, like $\alpha-$relaxation, the short-time particle motions were also observed to be heterogeneous and cooperative in nature. Furthermore, the increasing fraction of overlapping τ_c- and $\tau_\beta-$clusters versus packing suggests a direct connection between dynamic heterogeneities at the two distinct timescales. While other groups have explored the growth of particular length scales with increased supercooling, *e.g.*, point-to-set length scales, ξ_{PTS} and dynamic correlation lengths, ξ_{dyn} [39, 41], these parameters are associated only with long-time structural relaxation. In the present work, we identified a different and new length scale, ξ, that depends upon the spatial separation of clusters of most-mobile particles across short- and long-timescales; ξ grows with increased supercooling and is suggestive of spatial correlation between spatiotemporal dynamics at short- and long-times. In future, it will be interesting to examine relationships between ξ and τ_β (or τ_c), and to check for generalizability of our findings across interaction potentials (both isotropic and anisotropic) and dimension (2-D, 3-D).

We are grateful for useful discussions with Peter Collings, Doug Durian, Zahra Fakhraai, Robert Riggleman, Srikanth Sastry, Rajesh Ganapathy, Hima Nagamanasa and Shreyas Gokhale. We also acknowledge financial support from the National Science Foundation through DMR16-07378, the MRSEC DMR-1720530 including its Optical Microscopy Shared Experimental Facility, and NASA through NNX13AL27G.

* Electronic address: mishrachandan23@gmail.com

[1] L. Berthier, G. Biroli, J.-P. Bouchaud, L. Cipelletti, and W. van Saarloos, *Dynamical Heterogeneities in Glasses, Colloids and Granular Materials* (Oxford University Press, Oxford, 2011).
[2] M. D. Ediger, Annu. Rev. Phys. Chem. **51**, 99 (2000).
[3] S. Gokhale, A. Sood, and R. Ganapathy, Adv. Phys. **65**, 363 (2016) and references therein.
[4] E. R. Weeks, J. C. Crocker, A. C. Levitt, A. Schofield, and D. A. Weitz, Science **287**, 627 (2000).
[5] P. G. Debenedetti, and F. H. Stillinger, Nature **410**, 259 (2001).
[6] C. K. Mishra, and R. Ganapathy, Phys. Rev. Lett. **114**, 198302 (2015).
[7] Z. Zhang, P. J. Yunker, P. Habdas, and A. G. Yodh, Phys. Rev. Lett. **107**, 208303 (2011).
[8] A. Latka, Y. Han, A. M. Alsayed, A. B. Schofield, A. G. Yodh, A. G. and P. Habdas, Europhys. Lett. **86**, 58001 (2009); Z. Brown, M. J. Iwanicki, M. D. Gratale, X. Ma, A. G. Yodh, and P. Habdas, Europhys. Lett. **115**, 68003 (2016).
[9] G. Adam and J. H. Gibbs, J. Chem. Phys. **43**, 139 (1965).
[10] W. van Megen, T. C. Mortensen, S. R. Williams, and J. Muller, Phys. Rev. E **58**, 6073 (1998).
[11] G. Brambilla, D. El Masri, M. Pierno, L. Berthier, and L. Cipelletti, G. Petekidis, and A. B. Schofield, Phys. Rev. Lett. **102**, 085703 (2009).
[12] J. E. Hallett, F. Turci, and C. P. Royall, Nature Communications **9**, 3272 (2018).
[13] G. Biroli, J.-P. Bouchaud, K. Miyazaki, and D. R. Reichman, Phys. Rev. Lett. **97**, 195701 (2006).
[14] S. Karmakar, C. Dasgupta, and S. Sastry, Phys. Rev. Lett. **116**, 085701 (2016).
[15] K. L. Ngai, J. Chem. Phys. **109**, 6982 (1998).
[16] K. L. Ngai, Philosophical Magazine, **84(13-16)**, 1341 (2004).
[17] S. Capaccioli, K. L. Nga, M. Shahin Thayyil, and D. Prevosto, J. Phys. Chem. B **119(28)**, 8800 (2015); K. L. Ngai, S. Capaccioli, D. Prevosto, and L. M. Wang, J. Phys. Chem. B **119(38)**, 12502 (2015); K. L. Ngai, S. Capaccioli, D. Prevosto, and L. M. Wang, J. Phys. Chem. B **119(38)**, 12519 (2015);
[18] K L Ngai, J. Phys.: Condens. Matter **15**, S1107 (2003).
[19] K. L. Ngai, *Relaxation and diffusion in complex systems* (Springer Science & Business Media, 2011).
[20] L. Larini, A. Ottochian, C. D. Michele, and D. Leporini, Nature Phys. **4**, 42 (2008).
[21] U. Buchenau and R. Zorn, Eur. Phys. Lett. **18**, 523 (1992).
[22] M. T. Cicerone and J. F. Douglas, Soft Matter, **8**, 2983, (2012).
[23] R. Das, I. Taha, and S. Karmakar, J. Chem. Phys. **149**, 024501 (2018).

[24] A. Widmer-Cooper, H. Perry, P. Harrowell, and D. R. Reichman, Nature Phys. **4**, 711 (2008).

[25] F. W. Starr,S. Sastry, J. F. Douglas, and S. C. Glotzer, Phys. Rev. Lett. **89**, 125501 (2002).

[26] A. Widmer-Cooper and P. Harrowell, Phys. Rev. Lett. **96**, 185701 (2006).

[27] H. Tong, and H. Tanaka, Phys. Rev. X **8**, 011041 (2018).

[28] W. van Megen and S. M. Underwood, Phys. Rev. E **49**, 4206 (1994)].

[29] M. Fuchs, W. Göotze, S. Hildebrand, and A. Latz, J. Phys.: Condens. Matter **4**, 7709 (1992).

[30] J. Perez and J. Y. Cavaille, J. Non-Crystalline Solids, **172-174**, 1028 (1994).

[31] See Supplemental Material for the variation of four-point susceptibility χ_4 with probing-length Δa, algorithm to identify most-mobile particle clusters, morphology of clusters of most-mobile particles, the nature of overlap of $\tau_\beta-$clusters with τ_c-clusters and the check on aging effects.

[32] J. C. Crocker, and D. G. Grier, J. Colloid Interface Sci. **179**, 298 (1996).

[33] C. K. Mishra, P. Habdas, and A. G. Yodh, J. Phys. Chem. B **123(24)**, 5181 (2019).

[34] W. Kob and H. C. Andersen, Phys. Rev. Lett. **73**, 1376 (1994).

[35] C. K. Mishra, A. Rangarajan, and R. Ganapathy, Phys. Rev. Lett. **110**, 188301 (2013).

[36] C. Dasgupta, A. V. Indrani, S. Ramaswamy, and M. K. Phani, Europhys. Lett., **15(4)**, (1991).

[37] C. Donati, S. C. Glotzer, and P. H. Poole, Phys. Rev. Lett. **82**, 5064 (1999).

[38] A. S. Keys, *et al.*, Nature Phys. **3**, 260 (2007).

[39] K. H. Nagamanasa, S. Gokhale, A. K. Sood, and R. Ganapathy, Nature Phys. **11**, 403 (2015).

[40] R. Candelier, O. Dauchot, and G. Biroli, Phys. Rev. Lett. **102**, 088001 (2009).

[41] W. Kob, S. R-Vargas, and L. Berthier, Nature Phys. **8**, 164 (2012).